Internal dosimetry through GATE simulations of preclinical radiotherapy using a melanin-targeting ligand

2014 Phys. Med. Biol. 59 2183

(http://iopscience.iop.org/0031-9155/59/9/2183)

IOP Publishing | Institute of Physics and Engineering in Medicine Physics in Medicine and Biology

Phys. Med. Biol. **59** (2014) 2183–2198 doi:10.1088/0031-9155/59/9/2183

Internal dosimetry through GATE simulations of preclinical radiotherapy using a melanin-targeting ligand

Y Perrot[1], F Degoul[2,3], P Auzeloux[2,3], M Bonnet[2,3,4], F Cachin[2,3], J M Chezal[2,3], D Donnarieix[1,5], P Labarre[2,3], N Moins[2,3], J Papon[2,3], L Rbah-Vidal[2,3], A Vidal[2,3], E Miot-Noirault[2,3] and L Maigne[1]

[1] Clermont Université, CNRS/IN2P3, Laboratoire de Physique Corpusculaire de Clermont-Ferrand (LPC), F-63177 Aubière, France
[2] Imagerie Moléculaire et Thérapie Vectorisée, Clermont Université, Université d'Auvergne, F-63005 Clermont-Ferrand, France
[3] INSERM, UMR990, F-63005 Clermont-Ferrand, France
[4] IUT, Université d'Auvergne, Aubière, France
[5] Centre Jean Perrin, Service de Physique médicale, 58 rue Montalembert, F-63011 Clermont-Ferrand cedex, France

E-mail: maigne@clermont.in2p3.fr

Received 24 July 2013
Accepted for publication 28 February 2014
Published 8 April 2014

Abstract

The GATE Monte Carlo simulation platform based on the Geant4 toolkit is under constant improvement for dosimetric calculations. In this study, we explore its use for the dosimetry of the preclinical targeted radiotherapy of melanoma using a new specific melanin-targeting radiotracer labeled with iodine 131. Calculated absorbed fractions and *S* values for spheres and murine models (digital and CT-scan-based mouse phantoms) are compared between GATE and EGSnrc Monte Carlo codes considering monoenergetic electrons and the detailed energy spectrum of iodine 131. The behavior of Geant4 standard and low energy models is also tested. Following the different authors' guidelines concerning the parameterization of electron physics models, this study demonstrates an agreement of 1.2% and 1.5% with EGSnrc, respectively, for the calculation of *S* values for small spheres and mouse phantoms. S values calculated with GATE are then used to compute the dose distribution in organs of interest using the activity distribution in mouse phantoms. This study gives

the dosimetric data required for the translation of the new treatment to the clinic.

Keywords: targeted radiotherapy, melanoma, dosimetry, Monte Carlo, GATE

(Some figures may appear in colour only in the online journal)

1. Introduction

Targeted radiotherapy is an alternative approach to overcome the lack of effective treatments of melanoma. In this context, new radiopharmaceuticals have been developed to achieve much more selective treatments by keeping toxicity to a minimum. Since melanin pigment is detected in more than 90% of primary melanomas (Koch and Lange 2000) and in 50% of metastases (Nikkola *et al* 2002, Ghanem *et al* 2005), many melanoma-targeted strategies have been developed over the last decades both for diagnosis and/or for therapeutic purposes. Those are based on melanin-binding molecules such as polycyclic aromatic compounds, e.g. methylene blue or iodobenzamide analogues (Link and Carepenter 1992, Link *et al* 1998, Moins *et al* 2002, Chezal *et al* 2008). Among them, a radiolabeled melanin-targeting ligand (i.e. an [^{125}I]-*N*-(2-diethylaminoethyl)-6-iodoquinoxaline-2-carboxamide dihydrochloride salt named [^{125}I]ICF01012), has been selected for exhibiting a high, specific and long-lasting uptake in melanoma tumors (Chezal *et al* 2008). Regarding the encouraging effectiveness of ^{131}I-labeled ICF01012 for the therapeutic targeting of melanin-positive melanoma in preclinical models, a short-term phase 1 study is planned (Degoul *et al* 2013). It is in this context that studies on rodents are being performed with the aim of estimating the ratio between efficacy and toxicity. With the knowledge of [^{125}I]ICF01012 kinetic data previously published (Chezal *et al* 2008) and extrapolated to [^{131}I]ICF01012 (Bonnet-Duquennoy *et al* 2009, Degoul *et al* 2013), we performed a Monte Carlo (MC) dosimetric study on mice using the MIRD methodology (Loevinger *et al* 1991) in order to calculate the absorbed dose to sensitive organs and the tumor.

MC codes have been used to compute reference dosimetric quantities on realistic mouse geometries such as the mean absorbed dose per decay—namely the *S* value (Kolbert *et al* 2003, Stabin *et al* 2006, Bitar *et al* 2007, Larsson *et al* 2007). The GATE MC simulation platform (Jan *et al* 2004, 2011), based on the Geant4 toolkit (Agostinelli *et al* 2003), has not been used widely for nuclear medicine therapy, but has been used much more in the fields of imaging and quantitation. To the best of our knowledge, just two preclinical dosimetric studies involving fluorine 18 compounds have been already performed with GATE (Taschereau and Chatziioannou 2007, Mauxion *et al* 2013), and it is worth mentioning that recent developments (Jan *et al* 2011) have made GATE the first Monte Carlo platform able to handle both simulations of imaging and therapy modalities in the same framework. In this respect, a thorough evaluation of the code's dosimetric accuracy is needed, especially when using electron sources such as iodine 131. In a previous paper, we validated GATE/Geant4 for the production of accurate dose distributions using monoenergetic electrons from 50 keV to 20 MeV in agreement with EGSnrc or MCNP4C (Maigne *et al* 2011). Here, we explore the ability of GATE to compute the dosimetric quantities of interest through a realistic preclinical study of targeted radiation therapy using [^{131}I]ICF01012. Therefore, we first investigate the accuracy of GATE in comparison to EGSnrc, which is, up to now, well validated for electron dose calculations. Then, we calculate *S* values on digital and CT-scan-based mouse phantoms in order to estimate the absorbed dose to the organs of interest. These investigations highlight several issues of

Table 1. The relevant physics parameters of Geant4 version 9.5 (recommended and default values).

	Parameter	Recommended value	Default value
Ionization process	Max. fractional energy loss per step	0.2	0.2
	Max. range of particles whose steps have to be limited	0.1 mm	1 mm
Multiple scattering	MSC model	Urban95	Urban95
	Tracking algorithm	*Distance To boundary*	*Safety*
	Skin	1	–
Other options	dE/dx table binning	220	84
	Mean free path table binning	220	84

general interest to physicists who are interested in the internal dosimetry of beta emitters and are willing to use GATE.

2. Materials and methods

2.1. Monte Carlo simulation setup

2.1.1. GATE simulation setup. The present work was performed with version 6.2 of the GATE generic Monte Carlo platform (Jan *et al* 2011). This version of GATE makes use of Geant4 (Agostinelli *et al* 2003) version 9.5.p01.

Standard versus low energy physics package of Geant4. Within Geant4, electromagnetic physics can be implemented through standard or low energy models. It is the responsibility of users to correctly choose the physics adapted to its application, even if guidelines have been provided by the collaboration (see the next section).

The Geant4 standard electromagnetic physics package (Geant4 Collaboration 2010) describes hadronic and electromagnetic interactions for energies down to 990 eV and up to 100 TeV. Those physics models, developed to simulate high-energy physics experiments, are based on the parameterization of experimental data reaching an optimal efficiency between accuracy and computation time.

Low energy models, namely Livermore or Penelope, are additional models to extend the validity range of electromagnetic processes for photons, electrons and positrons at lower energies, down to a few hundred eV. They make use of shell cross-section data and are able to simulate fluorescence, Auger production and atomic relaxation. Livermore models are based on evaluated data libraries for photons and electrons, whereas positrons are handled by an analytical approach. Penelope models are still under development and were not studied in this paper.

It has to be noted that standard and low energy packages all use the same multiple scattering (MSC) model, Urban95 (Ivanchenko *et al* 2010).

For this study, we made comparisons between standard and low energy physics models.

Electron transport parameters. Whichever model is used, standard or low energy, step size limitations for charged particles are recommended for applications requiring higher accuracy for electron, hadron and ion tracking without magnetic fields. Table 1 summarizes the default and recommended values of parameters used for particle tracking (Ivanchenko *et al* 2011).

During the ionization process, the step size is limited so that it does not allow the decrease of the stopping range by more than 20%, until the range of the particle becomes lower than 100 μm (1 mm by default). The Geant4 MSC algorithm (Ivanchenko *et al* 2010) imposes additional step size limitations when tracking the charged particles. By default, the tracking algorithm restricts the step size when the particle enters a new volume to ensure a minimum of steps in any volume (*UseSafety* option). A further restriction allows switching to a single scattering mode near geometrical boundaries (*Distance To Boundary* option) in order to increase the accuracy of the simulation in a small region (the thickness defined by the '*skin*' parameter) near a boundary. Note that the binning option to construct stopping power and mean free path tables from 100 eV to 10 TeV is only of relevance for ion and hadron transport (Grevillot *et al* 2010). The effect of those electron transport parameters on the dose calculation is discussed in (Maigne *et al* 2011). Moreover, GATE inherits Geant4 capabilities to set the electromagnetic physics processes, thresholds for the production of secondary particles and maximum step size. For this work, the recommended parameters (see table 1) were selected and the production threshold for secondary particles (electrons, and photons) was set to 2 μm, whereas the maximum step size was restricted to 10 μm.

Voxelized phantom and source. Regarding targeted radiation therapy simulations, it is convenient to represent the phantom geometry and the distribution of primary particles by the mean of voxelized images derived from imaging facilities: CT scans to describe the attenuation map and SPECT or PET to describe the activity distribution. The downside of this method is the use of a large number of voxels involving time consumption for their management in Monte Carlo simulations if no improvement is done on particle tracking for such a specific geometry.

To answer this issue, Geant4 offers different ways to represent the attenuation map and to optimize the tracking of particles in voxelized geometries, as described in Sarrut and Guigues (2008). The nested parameterization or the region-oriented methods are the most convenient methods for radiation therapy applications (Sarrut and Guigues 2008). In this regard, the stoichiometric calibration described by Schneider *et al* (2000) is implemented in GATE to convert voxel values to materials (Jan *et al* 2011). Up to now, DICOM images are not yet readable using GATE and have to be converted in other formats such as Analyze or MetaImage formats. The GATE collaboration proposes to users the free software VV (Seroul and Sarrut 2008) to easily convert medical images. The description of activity maps is performed using an equivalent process—Interfile medical images are converted into activity maps using a simplified text file for the description of activity range values.

2.1.2. EGSnrc simulation setup. For validation purposes, the well-known Monte Carlo code EGSnrc (Kawrakow 2000a, 2000b) was used as a reference. It uses a condensed history approach based on the formalism developed by Kawrakow and Bielajew (1998) to sample angular distributions from the any-angle form of the screened Rutherford cross section. The resulting step-size independent electron transport algorithm, named Presta II, integrates the exact boundary crossing algorithm, which overcomes interface artifacts by switching to single scattering mode when the particle comes closer to a boundary (Kawrakow 2000a). As a result, EGSnrc has become the gold standard by passing the Fano cavity test for arbitrary electron step sizes and by reproducing an ion chamber response without artifacts in its electron transport algorithm (Kawrakow 2000b). To track particles, we applied the PRESTA II electron-step algorithm and the EXACT boundary crossing algorithm. Electron and photon tracking cuts, respectively ECUT and PCUT, were set to 521 and 1 keV. Here, simulations were

performed using egspp, the EGSnrc C++ class library (Kawrakow *et al* 2009). This extension provides libraries to write EGSnrc user code in C++ so that users can easily extend geometry and source packages.

2.2. S value calculations for small spheres

2.2.1. Absorbed fraction for monoenergetic electrons. In order to validate the accuracy of GATE to compute the energy deposited by low energy electrons and photons (<1 MeV), calculations of absorbed fractions for self-absorption were performed and compared with published data and EGSnrc simulations.

First, we compared our results with those published by Stabin and Konijnenberg (2000). The absorbed fractions for electrons and photons were computed in spheres of unit density and tissue equivalent medium located in a large scattering medium. Primary particles were isotropically and uniformly emitted within the spheres. For electrons, results were obtained for energies of 100 keV (144.4 μm CSDA range), 200 keV (453.0 μm CSDA range), 400 keV (1300 μm CSDA range) and 1 MeV (4410 μm CSDA range) and spheres of radius from 1.3 to 9.8 mm. For photons, results were obtained for energies of 30, 80, 364 and 662 keV in spheres of radius from 6.2 to 16.84 mm, since photons are more penetrating in the medium.

We also computed absorbed fractions in liquid water spheres (1.0 g cm^{-3}) of radius ranging from 10 μm to 10.0 mm for photons and electrons using the same source distribution. For radii greater than 10.0 mm, electrons are considered as non-penetrating, whereas for radii lower than 10 μm, the use of MC condensed history becomes questionable. The energies of electrons ranged from 10 keV (2.515 μm CSDA range) to 1 MeV (4367 μm CSDA range) and the energies of photons ranged from 4 to 650 keV.

For both calculations (in tissue equivalent medium and in liquid water), 2.5×10^6 electrons were generated per simulation resulting in a statistical uncertainty not exceeding 0.06%, and 10.0×10^6 photons were simulated to get a statistical uncertainty lower than 0.2%.

2.2.2. S values for 131 iodine source. As a second preliminary validation, we computed *S* values for small spheres of liquid water with an iodine 131 source uniformly distributed, according to the conditions of Bardiès and Chatal (1994). *S* values were computed by simulating an iodine 131 emission spectrum as presented in Champion *et al* (2008). Thus, the whole beta spectrum (from 10 to 766 keV) and the relevant discrete emissions (internal conversion electrons and Auger electrons) characteristic of iodine 131 were considered in all simulations.

2.3. S values calculations for murine phantoms

2.3.1. Digital versus CT-scan-based phantoms. The MOBY whole-body mouse phantom (Segars *et al* 2004) represents a 33 g, normal 16-week-old male C57BL6 mouse. The phantom is modeled as a three-dimensional rectangular array of $128 \times 128 \times 450$ cubic voxels of $250 \times 250 \times 250$ μm^3 (see figure 1(a)). In order to model the melanoma tumor, a spherical shape of 7.5 mm in diameter located on the right side of the mouse is added (using the inherent functionalities provided by the software). In addition, two spheres of 3.4 mm in diameter represent both eyes. The densities and elemental compositions of the organs were considered similar to human tissues. Four materials were defined (ICRU 1989): soft tissue (1.0 g cm^{-3}), lung (0.26 g cm^{-3}), bone (1.85 g cm^{-3}) and air (1.25 mg cm^{-3}). The masses of the organs are detailed in table 2.

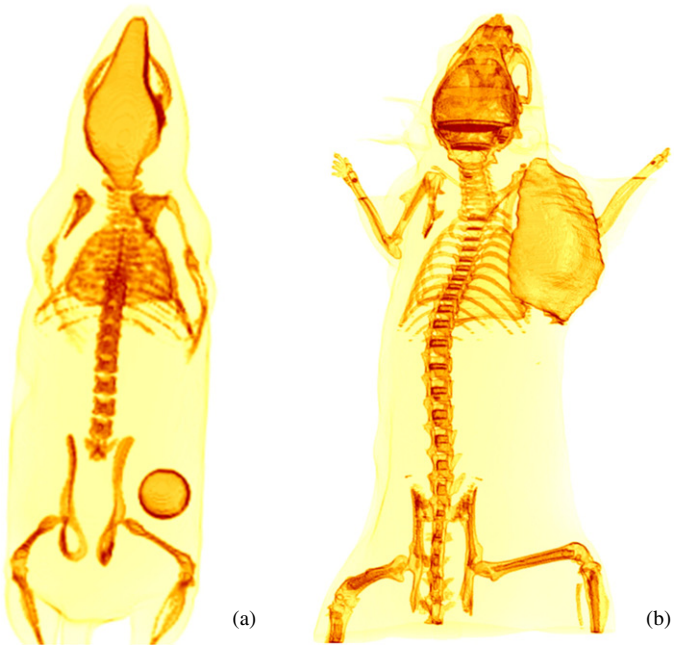

Figure 1. 3D views of (a) a MOBY phantom with a spherical tumor modeled on the right side and (b) a CT-scan-based phantom with the tumor located on the shoulder.

Table 2. Organ masses of murine models (MOBY and CT scans).

Organs	MOBY phantom (g)	CT-scan phantom (g)
Melanoma	2.0×10^{-01}	2.8×10^{-01}
Thyroid	5.0×10^{-04}	3.0×10^{-04}
Eyes	1.5×10^{-02}	1.4×10^{-02}
Liver	5.9×10^{-01}	5.8×10^{-01}
Kidneys	3.0×10^{-01}	1.8×10^{-01}
Lungs	1.5×10^{-01}	1.2×10^{-01}

Mouse phantoms were also modeled using CT scans (figure 1(b)). CT scans of C57BL6 mice were acquired using an Explore CT 120 MicroCT (GE Healthcare). Acquisition consisted of 360 views collected in one full gantry rotation, with a 20 ms exposure/view and x-ray tube settings of 100 kV and 50 mA. A modified Feldkamp's filtered back-projection algorithm was used to reconstruct a 3D volume with $200 \times 450 \times 900$ voxels with a voxel size of 98.85 μm. The ISOgray treatment planning system (TPS) was then used to contour the organs of interest in the reconstructed CT mouse volume. Tumor, eyes, bones, lung, kidneys, liver and thyroid were contoured. The Dicom RT-Struct file that was generated was then converted into adapted file readable by GATE (using Analyze for the geometry and Interfile for the activity distribution) or EGSnrc (for binary images) with a dedicated program. We applied the same densities and atomic compositions for organs as chosen for the MOBY phantom. The organ masses are listed in table 2. For the simulations, the MOBY and CT-scan-based phantoms were identically defined in EGSnrc and GATE in terms of voxel size and material definition.

2.3.2. S value calculations for 131 iodine source. *S* value calculations were performed for each organ listed in table 2. For each organ, a simulation was performed to compute the *S* value

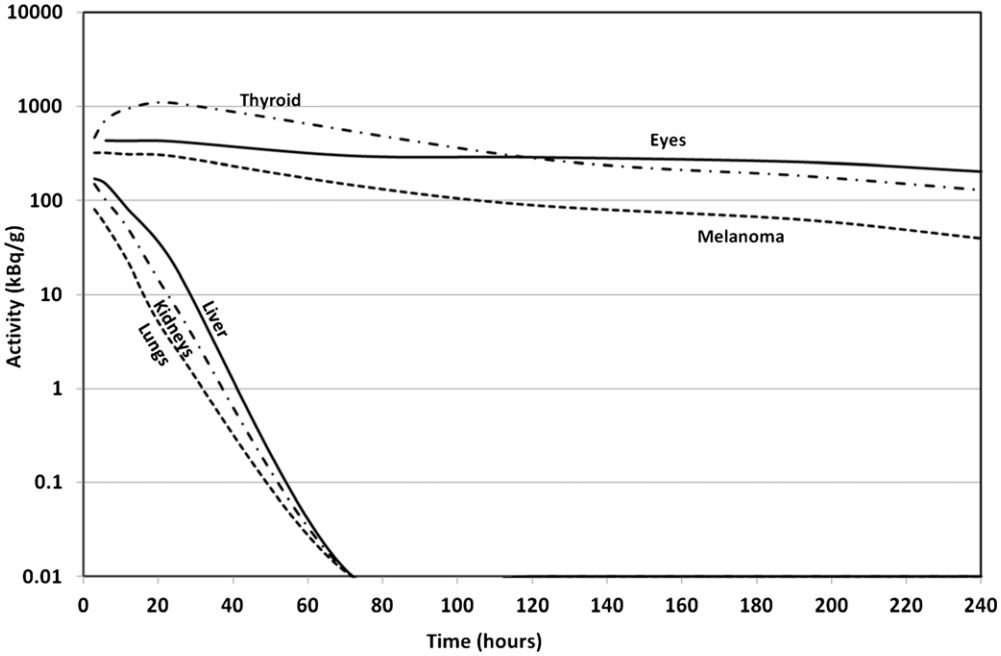

Figure 2. Time–activity curves of [^{125}I]ICF01012 extracted from measurements (Degoul *et al* 2013).

using a uniform distribution of iodine 131, emitting both electrons, according to the spectrum previously presented, and characteristic gamma and x-ray radiations, according to ICRP 38 nuclear data (ICRP 1983).

2.4. Dose distribution applied using ^{131}I-labeled ICF01012

2.4.1. Data acquisition set up. The cumulative activity of [^{131}I]ICF01012 for each organ of interest was estimated from [^{125}I]ICF01012 pharmacokinetics (Degoul *et al* 2013). The ^{125}I-labeled ICF01012 radiotracer biodistribution was evaluated in ten male black mice C57BL6 of approximately 24 g (Iffa-Credo, France) bearing a B16F0 primary melanoma tumor from whole body autoradiography using a digital autoradiographic analyzer AMBIS 4000 (Scanalytics, CSPI, San Diego, CA). Two mice were euthanized at 1 h, 6 h, 24 h, 5 days and 8 days after intravenous administration of 1.7 MBq of [^{125}I]ICF01012. Sagittal cryosections of 40 μm were used for measurements of the activity in the following organs: tumor, eyes, liver lungs, kidneys and thyroid. Given the highly sensitive linear response of the detector, the measured activity (cpm mm^{-2}) was converted into specific activity (kBq g^{-1}) using the calibration curve established for iodine 131. The specific activity was measured for each organ from 2 to 20 slices. The final specific activity for each organ is the result of the average activity obtained for two mice. Time–activity curves of [^{125}I]ICF01012 (Degoul *et al* 2013) are presented in figure 2. No fit has been used for the representation of time–activity curves, only a line connecting measured activity points.

2.4.2. Effective periods and cumulated activity calculations. The [^{125}I]ICF01012 biodistributions for each organ were fitted by a mono-exponential function to estimate the initial activity and the effective period of the radiotracer. Knowledge of the effective period

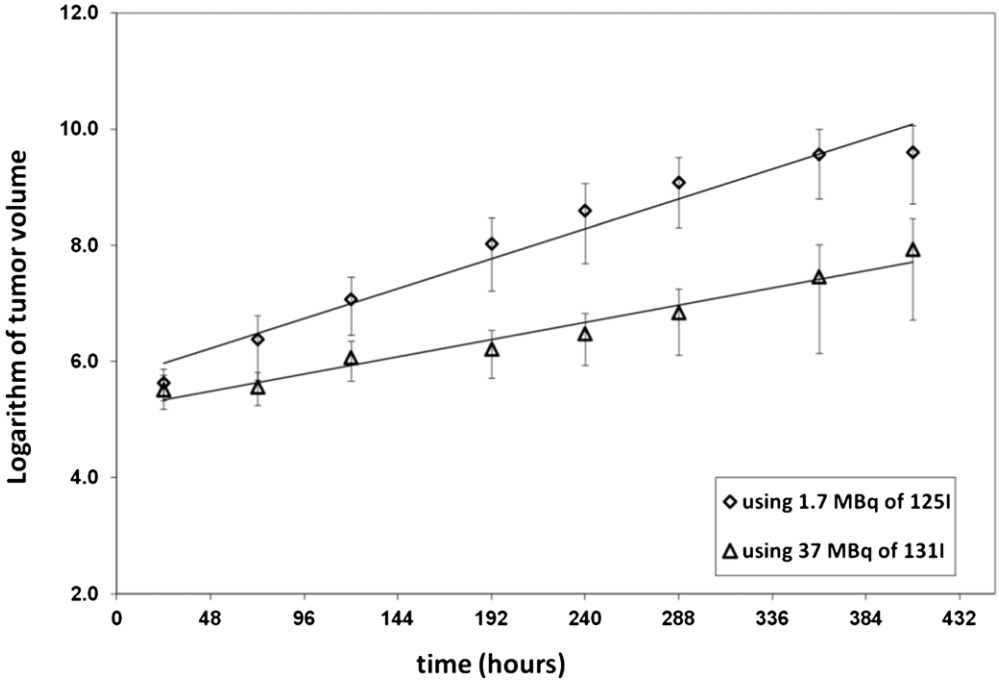

Figure 3. Tumor volume evolution as a function of time.

allowed us to estimate the biological period of [^{125}I]ICF01012. Then, the effective period of [^{131}I]ICF01012 for each organ was computed by taking into account the same biological period as [^{125}I]ICF01012. For the tumor, the biological period of [^{131}I]ICF01012 was corrected by a factor describing the exponential tumor volume evolution as a function of time, following the work of Mehrara *et al* (2007). Effectively, after the injection of 37 MBq of [^{131}I]ICF01012, the tumor growth was significantly reduced compared to the use of 1.7 MBq of [^{125}I]ICF01012, as shown in figure 3. With the assumption of a constant tumor density, the biological disappearance constant of [^{131}I]ICF01012 was corrected by a differential growth constant λ_m, as shown in equations (1) and (2):

$$\Delta\lambda_m = \lambda_m 125_I - \lambda_m 131_I \tag{1}$$

$$\lambda_{\text{bio}} 131_I = \lambda_{\text{bio}} 125_I - \Delta\lambda_m \tag{2}$$

where $\Delta\lambda_m$ is the differential growth constant, $\lambda_m 125_I$ and $\lambda_m 131_I$ are the growth constants obtained by mono-exponential fits of the evolution of the tumor volume as a function of time when using, respectively, ^{125}I and ^{131}I, and $\lambda_{\text{bio}} 125_I$ and $\lambda_{\text{bio}} 131_I$ are the biological decays for [^{125}I]ICF01012 and [^{131}I]ICF01012, respectively.

The cumulative activity of [^{131}I]ICF01012 was computed for a therapeutic activity of 37 MBq.

3. Results and discussion

3.1. S value calculations for small spheres

Tables 3 and 4 present absorbed fractions calculated respectively for electrons and photons computed with GATE, making use of the standard physics package and recommended physics

Table 3. Absorbed fractions for electrons in spheres made of tissue equivalent medium calculated with EGS4 (Stabin and Konijnenberg 2000), GATE using standard physics package option 3 and EGSnrc.

Sphere radius (mm)	EGS4 (Stabin and Konijnenberg 2000)	GATE	EGSnrc	GATE/ EGS4	EGSnrc/ EGS4	GATE/ EGSnrc
			Energy (MeV) 0.1			
1.3	0.962	0.957	0.957	0.995	0.995	1.000
2.9	0.982	0.981	0.981	0.999	0.999	1.000
4.9	0.989	0.989	0.988	1.000	0.999	1.000
6.2	0.992	0.991	0.991	0.999	0.999	1.000
7.8	0.993	0.993	0.993	1.000	1.000	1.000
9.8	0.994	0.994	0.994	1.000	1.000	1.000
			Energy (MeV) 0.2			
1.3	0.864	0.868	0.869	1.004	1.005	0.999
2.9	0.937	0.940	0.941	1.003	1.004	1.000
4.9	0.962	0.964	0.964	1.002	1.003	1.000
6.2	0.971	0.972	0.972	1.001	1.001	1.000
7.8	0.976	0.977	0.977	1.001	1.001	1.000
9.8	0.982	0.982	0.982	1.000	1.000	1.000
			Energy (MeV) 0.4			
1.3	0.644	0.638	0.642	0.991	0.996	0.994
2.9	0.832	0.832	0.834	1.000	1.002	0.998
4.9	0.900	0.900	0.901	1.000	1.001	0.999
6.2	0.921	0.920	0.921	0.999	1.000	0.999
7.8	0.936	0.936	0.937	1.001	1.001	0.999
9.8	0.948	0.949	0.950	1.001	1.002	0.999
			Energy (MeV) 1.0			
1.3	0.196	0.197	0.196	1.006	1.000	1.006
2.9	0.487	0.491	0.494	1.007	1.013	0.994
4.9	0.680	0.680	0.682	1.001	1.003	0.997
6.2	0.742	0.744	0.746	1.003	1.005	0.998
7.8	0.794	0.795	0.796	1.001	1.003	0.998
9.8	0.834	0.835	0.837	1.002	1.003	0.998

parameters listed in table 1. Ratios between the data are given to better compare the results. Even if the good agreement for low energy electrons is to be linked to the high values of absorbed fractions, the different codes give similar results, even for higher energies in the smallest spheres. For photons, while differences are acceptable between GATE and EGSnrc, disagreements exceeding 4% are found between GATE and the data of Stabin *et al* obtained with EGS4. Differences between the codes may come from different cross-section tables or particle transport methods.

Tables 5 and 6 present absorbed fractions calculated respectively for electrons and photons in spheres made of liquid water. For both particle types, GATE and EGSnrc are in good agreement. For electrons, the largest differences found for spheres of radius much smaller than the electron range may illustrate differences in the electron transport method used in the codes. Nevertheless, those differences do not exceed 1.2%.

Table 7 gives comparisons of S values using an iodine 131 spectrum for different sphere sizes between GATE (using the same physics as for previous tables), EGSnrc and Bardiès and Chatal results, who integrated numerically the point kernels of Berger calculated with the MC code ETRAN (Bardiès and Chatal 1994). The largest discrepancy between GATE and EGSnrc does not exceed 0.8%. Between GATE and the values of Bardiès and Chatal, the

Table 4. Absorbed fractions for electrons in spheres made of tissue equivalent medium calculated with EGS4 (Stabin and Konijnenberg 2000), GATE using standard physics package option 3 and EGSnrc.

Sphere radius (mm)	EGS4 (Stabin and Konijnenberg 2000)	GATE	EGSnrc	GATE/ EGS4	EGSnrc/ EGS4	GATE/ EGSnrc
			Energy (MeV) 0.03			
6.2	0.065	0.068	0.069	1.046	1.062	0.985
9.85	0.105	0.112	0.111	1.064	1.055	1.008
13.37	0.143	0.151	0.151	1.057	1.054	1.003
16.84	0.179	0.189	0.189	1.057	1.056	1.001
			Energy (MeV) 0.08			
6.2	0.012	0.013	0.013	1.043	1.046	0.997
9.85	0.020	0.021	0.021	1.046	1.035	1.011
13.37	0.028	0.029	0.029	1.046	1.034	1.012
16.84	0.037	0.038	0.038	1.025	1.018	1.007
			Energy (MeV) 0.364			
6.2	0.015	0.015	0.015	0.979	0.985	0.994
9.85	0.023	0.024	0.024	1.033	1.027	1.005
13.37	0.032	0.032	0.032	1.010	1.007	1.003
16.84	0.040	0.041	0.041	1.024	1.021	1.003
			Energy (MeV) 0.662			
6.2	0.014	0.014	0.014	0.986	0.979	1.007
9.85	0.022	0.023	0.022	1.032	1.022	1.010
13.37	0.031	0.031	0.031	1.009	1.000	1.009
16.84	0.039	0.040	0.039	1.016	1.008	1.008

largest difference is 1.0%. This agreement is consistent with the absorbed fractions previously shown.

3.2. Comparisons between physics models

Table 8 shows the influence of using Livermore models (low energy physics package) compared to standard models. No significant differences are found in S values for small spheres using an iodine 131 source between the two models, even for the smallest spheres. This means that neither the extension of processes down to a few hundred eV nor the fluorescence proposed by the Livermore models are relevant for an absorbed dose calculation at a geometrical scale down to 10 μm. Furthermore, the simulation time with Livermore models is around 27% longer than the computation time with standard models. To explain this difference, we have to keep in mind that Livermore models consider the fluorescence of excited atoms and have to interpolate databases to sample the state of a particle after each interaction, whereas standard models make use of an analytical approach. Therefore, we recommend using standard models when considering energy deposition in volumes of size superior to 10 μm.

3.3. S values calculation for mouse models

Table 9 shows S values computed with GATE and EGSnrc both for digital and CT-scan-based phantoms. Values include the self and crossed absorbed dose. Differences between the two codes do not exceed 1.5%. Differences observed between MOBY and CT-scan-based phantoms become more significant for the thyroid (3.0×10^{-4} g), for which the ranges of emitted electrons are not negligible compared to the dimensions of the organs, leading to

Table 5. Calculated absorbed fractions in liquid water for different sphere sizes computed with GATE using standard physics package option 3 for electrons with initial energies between 10 keV and 1.0 MeV.

	Energy							
	0.01 MeV		0.02 MeV		0.05 MeV		0.1 MeV	
Sphere radius (mm)	GATE	GATE/ EGSnrc	GATE	GATE/ EGSnrc	GATE	GATE/ EGSnrc	GATE	GATE/ EGSnrc
0.01	0.902	0.996	0.675	0.989	0.12	1.012	0.031	1.005
0.05	0.980	0.999	0.930	0.995	0.672	0.990	0.210	1.000
0.1	0.990	0.999	0.965	0.997	0.833	0.997	0.491	0.994
0.5	0.998	1.000	0.993	0.999	0.966	1.000	0.890	0.999
1.0	0.999	1.000	0.996	1.000	0.983	1.000	0.945	1.000
5.0	1.000	1.000	0.999	1.000	0.997	1.000	0.989	1.000
10.0	1.000	1.000	1.000	1.000	0.998	1.000	0.994	0.999
	0.2 MeV		0.4 MeV		0.6 MeV		1.0 MeV	
	GATE	GATE/ EGSnrc	GATE	GATE/ EGSnrc	GATE	GATE/ EGSnrc	GATE	GATE/ EGSnrc
0.01	0.01	0.992	0.004	0.995	0.002	0.995	0.001	0.992
0.05	0.054	1.001	0.019	0.992	0.011	0.995	0.006	0.992
0.1	0.119	1.003	0.040	0.999	0.023	0.997	0.013	0.997
0.5	0.670	0.998	0.260	1.002	0.132	0.999	0.069	1.001
1.0	0.831	0.999	0.545	0.991	0.314	0.998	0.146	0.998
5.0	0.965	1.000	0.902	0.998	0.832	0.996	0.688	0.994
10.0	0.981	0.998	0.946	0.995	0.909	0.993	0.842	1.000

Table 6. Calculated absorbed fractions in liquid water for different sphere sizes computed with GATE using standard physics package option 3 for photons with initial energies between 4 and 650 keV.

	Energy					
	0.004 MeV		0.03 MeV		0.08 MeV	
Sphere radius (mm)	GATE	GATE/ EGSnrc	GATE	GATE/ EGSnrc	GATE	GATE/ EGSnrc
5.0	0.982	1.000	0.060	0.991	0.010	1.003
10.0	0.991	1.000	0.121	0.992	0.022	0.998
15.0	0.994	0.999	0.180	1.002	0.034	1.002
20.0	0.995	1.000	0.236	0.991	0.047	1.005
	0.35 MeV		0.5 MeV		0.65 MeV	
	GATE	GATE/ EGSnrc	GATE	GATE/ EGSnrc	GATE	GATE/ EGSnrc
5.0	0.012	1.006	0.012	0.994	0.011	0.999
10.0	0.024	0.999	0.024	1.001	0.023	1.002
15.0	0.036	1.002	0.036	0.993	0.035	1.000
20.0	0.049	1.011	0.048	0.992	0.048	1.005

a crucial tracking of particles. Nevertheless, we can conclude that GATE and EGSnrc are in agreement. Discrepancies on *S* value calculations will not impact on the absorbed dose estimation regarding the uncertainty of cumulative activity. We therefore recommend using the standard physics package of Geant4 to compute the *S* values for beta emitters. We can be

Table 7. Calculated *S* values using GATE and EGSnrc, compared with Bardiès and Chatal (1994), for small spheres in liquid water using an ^{131}I source.

Sphere radius (mm)	*S* value GATE (Gy Bq^{-1} s^{-1})	*S* value EGSnrc (Gy Bq^{-1} s^{-1})	*S* value Bardiès–Chatal (Gy Bq^{-1} s^{-1})	GATE/ EGSnrc	GATE/ Bardiès–Chatal
0.01	1.61×10^{-04}	1.61×10^{-04}	1.61×10^{-04}	1.000	0.999
0.05	5.38×10^{-06}	5.41×10^{-06}	5.38×10^{-06}	0.994	1.000
0.1	1.19×10^{-06}	1.20×10^{-06}	1.20×10^{-06}	0.992	0.990
0.5	3.08×10^{-08}	3.10×10^{-08}	3.11×10^{-08}	0.995	0.990
1.0	5.31×10^{-09}	5.35×10^{-09}	5.35×10^{-09}	0.994	0.993
5.0	5.56×10^{-11}	5.56×10^{-11}	5.54×10^{-11}	0.999	1.003
10.0	7.16×10^{-12}	7.17×10^{-12}	7.13×10^{-12}	0.999	1.005

Table 8. Calculated *S* values for an ^{131}I source using Geant4 standard and low energy models.

Sphere radius (mm)	*S* value low energy (Gy Bq^{-1} s^{-1})	*S* value low energy/standard	Computation time low energy/standard
0.01	1.61×10^{-04}	1.004	1.24
0.05	5.42×10^{-06}	1.007	1.31
0.1	1.20×10^{-06}	1.008	1.26
0.5	3.08×10^{-08}	1.001	1.24
1.0	5.32×10^{-09}	1.001	1.29
5.0	5.56×10^{-11}	1.000	1.24
10.0	7.16×10^{-11}	1.000	1.28

Table 9. *S* values for two murine models: MOBY and the CT-scan-based phantom. Comparisons are between GATE and EGSnrc computations.

	S value: MOBY (Gy Bq^{-1} s^{-1})		*S* value: CT-scan phantom (Gy Bq^{-1} s^{-1})	
Organs	GATE	GATE/ EGSnrc	GATE	GATE/ EGSnrc
Melanoma	1.42×10^{-10}	0.999	9.97×10^{-11}	0.995
Thyroid	2.54×10^{-08}	0.988	4.01×10^{-08}	0.990
Eyes	1.41×10^{-09}	0.997	1.55×10^{-09}	1.001
Liver	5.58×10^{-11}	1.002	5.57×10^{-11}	0.998
Kidneys	8.45×10^{-11}	0.995	1.45×10^{-10}	0.996
Lungs	1.32×10^{-10}	0.989	1.62×10^{-10}	0.985

confident with the assertion that the computation of *S* values for human models should give the same level of accuracy.

3.4. Dosimetry for murine models

For clinical purposes, the information about the absorbed dose is mandatory to establish the relationship between the injected activity of [^{131}I]ICF01012 and the inhibition of the tumor growth. The absorbed dose to organs is calculated by multiplying the cumulative activity (see table 10) and *S* values (see table 9). Results for both murine models are presented in figure 4. As suggested in section 3.2, no relevant discrepancies are found between the two murine models. These results highlight several points about the efficiency of [^{131}I]ICF01012. First,

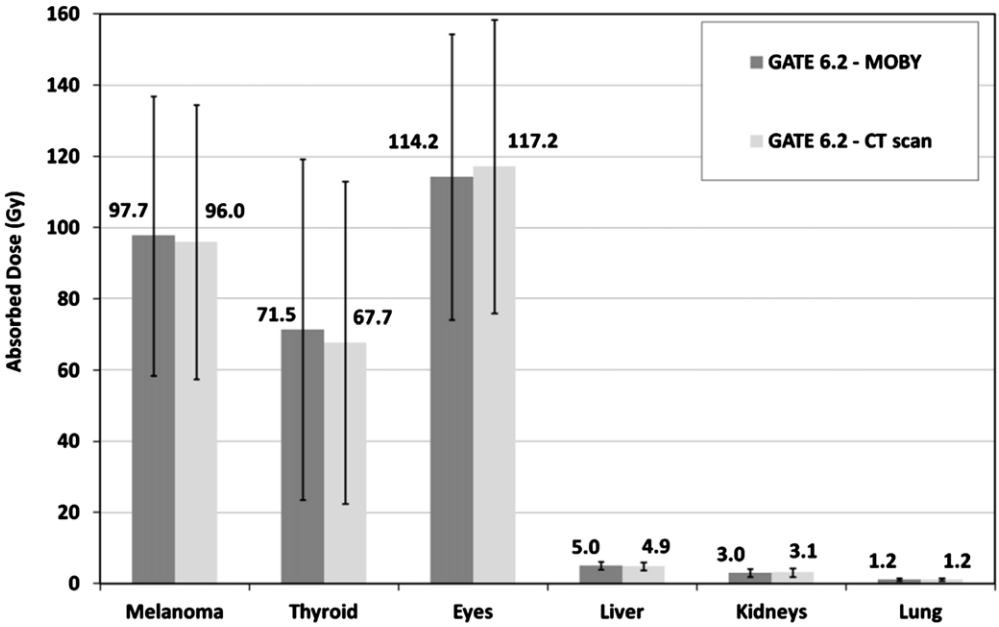

Figure 4. Comparisons of absorbed dose to organs after injection of 37 MBq of [^{131}I] ICF01012 for MOBY and CT-scan-based phantoms.

Table 10. Biological periods, effective periods and cumulative activity of [^{131}I] ICF01012 biodistributions for melanoma, thyroid, eyes, liver, kidneys and lungs.

Organs	^{131}I biological period (h)	^{131}I effective period (h)	^{131}I cumulative activity (Bq s kg^{-1})
Melanoma	150.6	84.5	3.44×10^{15}
Thyroid	101.9	66.6	5.63×10^{15}
Eyes	273.2	112.9	5.40×10^{15}
Liver	7.6	7.5	1.52×10^{14}
Kidneys	5.1	5.0	1.19×10^{14}
Lungs	4.4	4.3	6.19×10^{13}

the delivery of 96.0 Gy to the tumor is sufficient for an effective anti-tumor response, indeed it was demonstrated that 20 MBq of [^{131}I]ICF01012 delivering 30 Gy to B16BL6 tumors leads to a significant tumor progression decrease (Degoul *et al* 2013), whereas the dose delivery to major organs is low (<5 Gy). Secondly, some considerations concerning the impact of activity distribution in the eyes must be pointed out. Melanin content is mainly distributed in ciliary bodies and choroid (Durairaj *et al* 2012), which can be represented by a shell of thickness 10 μm around the mouse eye. If we consider an activity distribution located in the shell, we reach an absorbed dose of 8.2 Gy in the retina and 1.1 Gy in the eye.

4. Conclusion

GATE is the first Monte Carlo platform handling simulations of both imaging and therapy modalities in the same framework. GATE provides tools for dosimetry that can be used for the modeling of targeted radiation therapy studies. Among the features, GATE offers the

possibility to describe attenuation and activity maps directly from medical images. Even if images have to be converted in adapted formats (analyze for attenuation maps, Interfile for activity maps), the free software VV proposed by the GATE collaboration is convenient and user friendly. Real-time motion management for voxelized sources and phantoms, not explored in this study, allows GATE to produce personalized dosimetry in an easier way than with other codes. When high statistics are required, the distribution of GATE simulations among multiple resources, geographically distributed, is performed using the GateLab (Camarasu-Pop *et al* 2010) web platform (http://vip.creatis.insa-lyon.fr/). At last, the physics accuracy is checked at each release through benchmarks available to the community. In this work, we explore GATE features for providing a preclinical dosimetry for an innovative targeted radiotherapy using an ^{131}I-labeled melanin-targeting ligand. First, we showed that the accuracy of GATE using Geant4 standard models, in comparison with EGSnrc calculations and published data, is suitable for targeted radiotherapy applications involving electron sources with energies from 10 keV to 1 MeV when energy deposits are scored in volumes greater than 10 μm. That is why we recommend the use of standard models to compute *S* values for beta emitters in such conditions. As has been shown with the uptake of [^{131}I]ICF01012 in the eyes, radiopharmaceutical toxicity has to be properly defined for internal tissues (like the retina).

Acknowledgments

This work was supported by grants from Plan Cancer 2009–2013 French national initiative through the call for proposals 'Domaine de la physique, des mathématiques ou des sciences de l'ingénieur appliqués au Cancer' managed by INSERM (Institut National de la Santé et de la Recherche Médicale) under contract PC201116. The authors wish to thank the OpenGATE and Geant4 collaborations for their technical support. We also express our gratitude to Cyclopharma Laboratories, CLARA (Cancéropôle Lyon Rhône-Alpes Auvergne), the Auvergne Regional Council, the Puy de Dôme General Council, Clermont Community, the European Regional Development Fund, the European Union, The French Ligue contre le Cancer and the Bullukian Foundation for their financial support.

References

Agostinelli S *et al* 2003 Geant4—a simulation toolkit *Nucl. Instrum. Methods Phys. Res.* A **506** 250–303

Bardiès M and Chatal J F 1994 Absorbed doses for internal radiotherapy from 22 beta-emitting radionuclides: beta dosimetry of small spheres *Phys. Med. Biol.* **39** 961–81

Bitar A, Lisbona A, Thedrez P, Sai Maurel C, Le Forestier D, Barbet J and Bardiès M 2007 A voxel-based mouse for internal dose calculations using Monte Carlo simulations (MCNP) *Phys. Med. Biol.* **52** 1013–25

Bonnet-Duquennoy M *et al* 2009 Targeted radionuclide therapy of melanoma: anti-tumoural efficacy studies of a new ^{131}I labelled potential agent *Int. J. Cancer* **125** 708–16

Camarasu-Pop S, Glatard T, Mościcki J T, Benoit-Cattin H and Sarrut D 2010 Dynamic partitionning of GATE Monte Carlo simulations on EGEE *J. Grid Comput.* **8** 241–59

Champion C, Zanotti-Fregonara P and Hindié E 2008 CELLDOSE: a Monte Carlo code to assess electron dose distribution—*S* values for ^{131}I in spheres of various sizes *J. Nucl. Med.* **49** 151–7

Chezal J M *et al* 2008 Evaluation of radiolabeled (hetero)aromatic analogues of N-(2-diethylaminoethyl)-4-iodobenzamide for imaging and targeted radionuclide therapy of melanoma *J. Med. Chem.* **51** 3133–44

Degoul F *et al* 2013 *In vivo* efficacy of melanoma internal radionuclide therapy with ^{131}I-labelled melanin-targeting heteroarylcarboxamide molecule *Int. J. Cancer* **133** 1042–53

Durairaj C, Chastain J E and Kompella U B 2012 Intraocular distribution of melanin in human, monkey, rabbit, minipig and dog eyes *Exp. Eye Res.* **98** 23–27

Geant4 Collaboration 2010 *Physics Reference Manual* (Version Geant4 9.4) http://geant4.cern.ch/support/userdocuments.shtml

Ghanem N, Altehoefer C, Hogerle S, Nitzsche E, Lorhmann C, Shafer O, Kotter E and Langer M 2005 Detectability of liver metastases in malignant melanoma: prospective comparison of magnetic resonance imaging and positron emission tomography *Eur. J. Radiol.* **54** 264–70

Grevillot L, Frisson T, Zahra N, Bertrand D, Stichelbaut F, Freud N and Sarrut D 2010 Optimization of Geant4 settings for proton pencil beam scanning simulations using GATE *Nucl. Instrum. Methods Phys. Res.* B **268** 3295–305

ICRP 1983 Radionuclide transformations—energy and intensity of emissions *Ann. ICRP* 11–13 *ICRP Publication* 38

ICRU 1989 Tissue substitutes in radiation dosimetry and measurement *ICRU Report* 44 (Bethesda, MD: ICRU)

Ivanchenko V N, Kadri O, Maire M and Urban L 2010 Geant4 models for simulation of multiple scattering *J. Phys.: Conf. Ser.* **219** 032045

Ivanchenko V *et al* 2011 Recent improvements in Geant4 electromagnetic physics models and interfaces *Prog. Nucl. Sci. Technol.* **2** 898–903

Jan S *et al* 2004 GATE: a simulation toolkit for PET and SPECT *Phys. Med. Biol.* **49** 4543–61

Jan S *et al* 2011 GATE V6: a major enhancement of the GATE simulation of the GATE simulation platform enabling modeling of CT and radiotherapy *Phys. Med. Biol.* **56** 881–901

Kawrakow I 2000a Accurate condensed history Monte Carlo simulation of electron transport: I. EGSnrc, the new EGS4 version *Med. Phys.* **27** 485–98

Kawrakow I 2000b Accurate condensed history Monte Carlo simulation of electron transport: II. Application to ion chamber response simulations *Med. Phys.* **27** 499–517

Kawrakow I and Bielajew A F 1998 On the representation of electron multiple elastic scattering distributions for Monte Carlo calculations *Nucl. Instrum. Methods Phys. Res.* B **134** 325–35

Kawrakow I, Mainegra-Hing E, Tessier F and Walters B R B 2009 The EGSnrc C++ class library *NRC Report* PIRS-898(revA) (Ottawa, Canada: NRC)

Koch S E and Lange J R 2000 Amelanotic melanoma: the great masquerader *J. Am. Acad. Dermatol.* **42** 731–4

Kolbert K S, Watson T, Matei C, Xu S, Koutcher J A and Sgouros G 2003 Murine S factors for liver, spleen and kidney *J. Nucl. Med.* **44** 784–91

Larsson E, Strand S E, Ljungberg M and Jönsson B A 2007 Mouse S-factors based on Monte Carlo simulations in the anatomical realistic Moby phantom for internal dosimetry *Cancer Biother. Radiopharm.* **22** 438–42

Link E M, Blower P J, Costa D C, Lane D M, Lui D, Brown R S D, Ell P J and Spittle M F 1998 Early detection of melanoma metastases with radioiodinated methylene blue *Eur. J. Nucl. Med.* **25** 1322–9

Link E M and Carepenter R N 1992 ^{211}At-methylene blue for targeted radiotherapy of human melanoma xenografts: treatment of cutaneous tumours and lymph node metastases *Cancer Res.* **52** 4385–90

Loevinger R, Budinger T F and Watson E E 1991 *MIRD Primer for Absorbed Dose Calculations* (New York: Society of Nuclear Medicine) pp 1–17

Maigne L, Perrot Y, Schaart D R, Donnarieix D and Breton V 2011 Comparison of GATE/Geant4 with EGSnrc and MCNP for electron dose calculations at energies between 15 keV and 20 MeV *Phys. Med. Biol.* **56** 811–27

Mauxion T, Barbet J, Suhard J M, Pouget J P, Poirot M and Bardiès M 2013 Improved realism of hybrid mouse models may not be sufficient to generate reference dosimetric data *Med. Phys.* **40** 052501

Mehrara E, Forssell-Aronsson E, Ahlman H and Bernhardt P 2007 Specific growth rate versus doubling time for quantitative characterization of tumor growth rate *Cancer Res.* **10** 3970–75

Moins N *et al* 2002 ^{123}I-N-(2-diethylaminoethyl)-2-iodobenzamide: a potential imaging agent for cutaneous melanoma staging *Eur. J. Nucl. Med. Mol. Imaging* **29** 1478–84

Nikkola J, Vihinen P, Vlaykova T, Hahka-Kemppinen M, Kahari V M and Pyrhonen S 2002 High expression levels of collagenase-1 and stromelysin-1 correlate with shorter disease-free survival in human metastatic melanoma *Int. J. Cancer* **97** 432–8

Sarrut D and Guigues L 2008 Region-oriented CT image representation for reducing computing time of Monte Carlo simulations *Med. Phys.* **35** 1452–63

Schneider W, Bortfeld T and Shlegel W 2000 Correlation between CT numbers and tissue parameters needed for Monte Carlo simulations of clinical dose distributions *Phys. Med. Biol.* **45** 459–78

Segars W P, Tsui B M W, Frey E C, Johnson G A and Berr S S 2004 Development of a 4D digital mouse phantom for molecular imaging research *Mol. Imaging Biol.* **6** 149–59

Seroul P and Sarrut D 2008 VV: Viewer for the evaluation of 4D image registration *Medical Image Computing and Computer-Assisted Intervention (MICCAI) Workshop* 1–8

Stabin M G and Konijnenberg M W 2000 Re-evaluation of absorbed fractions for photons and electrons in spheres of various sizes *J. Nucl. Med.* **41** 149–60

Stabin M G, Peterson T E, Holburn G E and Emmons M A 2006 Voxel-based mouse and rat models for internal dose calculations *J. Nucl. Med.* **47** 655–9

Taschereau R and Chatziioannou A F 2007 Monte Carlo simulations of absorbed dose in a mouse phantom from 18-fluorine compounds *Med. Phys.* **34** 1026–36